Available online at www.sciencedirect.com
SCIENCE DIRECT
Journal of Nuclear Materials 348 (2006) 243–255
journal of nuclear materials
www.elsevier.com/locate/jnucmat

Damage inhomogeneity in the core region of displacement cascades in simplified nuclear glasses

J.-M. Delaye *, D. Ghaleb

Commissariat à l'énergie atomique (CEA), Rhône Valley Research Center, DEN/DTCD/SECM/LCLT, BP 17171, 30207 Bagnols-sur-Cèze cedex, France

Received 21 June 2005; accepted 30 September 2005

Abstract

Displacement cascades at energies ranging from 16 keV to 70 keV were simulated by classical molecular dynamics. Damage inhomogeneity was observed in each case: the atomic density was diminished by the incident projectile to a variable extent depending on the regions concerned. The regions near the initial projectile position are largely annealed, and regions near the end of the cascade are relatively unaffected because of the low residual projectile energy. However, maximum damage occurs in intermediate regions from collisions with incident projectiles at energies ranging from about 10 keV to 25 keV. This phenomenon illustrates the competition between structure annealing and projectile-induced damage: both increase with the local energy, but with different dynamics. At the highest energies, annealing wins out over damage, restoring the glass structure to its pristine state; hence the good structural behaviour in the zones closest to the initial projectile position, which are subjected to the greatest local temperature rise.

PACS: 71.15Pd; 61.82Ms; 78.55Qr

1. Introduction

Nuclear glasses intended for disposal or interim storage of long-lived radioactive elements will be subjected to alpha, beta, gamma and heavy recoil nuclei irradiation resulting in both electronic excitation and atom displacements [1,2]. Work has been carried out for several years to simulate the effect of atomic displacement cascades in simplified glass models subjected to the passage of heavy projectiles [3,4].

Actinide recoil nuclei accelerated to energies between 70 keV and 100 keV dissipate about 90% of their energy through ballistic collisions [5]; this justifies the use of classical molecular dynamics [6], which is perfectly suitable for reproducing this type of collision [7,8].

Classical molecular dynamics allowed us to simulate cascades in the energy range from 0 keV to 25 keV; a recently developed method, CoMoD, combining two types of molecular dynamics, allowed us to reach realistic energies [9] corresponding to the deceleration of recoil nuclei arising from

* Corresponding author. Tel.: +33 4 66 79 17 94; fax: +33 4 66 79 66 20.
E-mail address: jean-marc.delaye@cea.fr (J.-M. Delaye).

0022-3115/$ - see front matter © 2005 Elsevier B.V. All rights reserved.
doi:10.1016/j.jnucmat.2005.09.025

alpha decay. The CoMoD method consists first in simulating the cascade morphology, i.e. all the atom displacements produced by the successive ballistic collisions, by computing only the collision sequences using very short range potentials. The resulting morphology is then subdivided into a set of elementary zones that are fully calculated by classical molecular dynamics; the kinetic and thermal conditions at the boundaries of each zone are taken from ballistic molecular dynamics calculations. These elementary calculations are used to reconstitute the entire cascade, reproducing the collision sequences and the subsequent relaxation phase.

All the simulated cascades involve two successive phases. Ballistic collisions between atoms during the first few tenths of a picosecond depolymerize the glass network. This is followed by a relaxation phase, which restores the structure to its initial mean configuration and is increasingly effective at high projectile energies. It has recently been observed that repolymerization is increasingly effective when the local energy deposition rate is high; this suggests that the damage induced by a primary projectile tends to accumulate in zones subjected to collisions by intermediate- or low-energy projectiles [10].

The purpose of this work was to pursue the analysis of structural damage produced by a heavy projectile, by discriminating the effects in the different regions of a cascade. At energies exceeding 16 keV, the cascade becomes sufficiently vast to distinguish the core region from the periphery, and thus to investigate spatial damage variations.

Section 2 describes the characteristics of molecular dynamics as used to simulate glass structures and displacement cascades; Section 3 analyzes both the local and overall results obtained for 25 keV and 70 keV cascades. The discussion in Section 4 situates these findings within the context of the current state of knowledge concerning irradiation effects in nuclear glass.

2. Methodology

2.1. Simulating cascades by classical molecular dynamics

Born–Mayer–Huggins potentials were used to simulate glass with the following molar composition: 63.8% SiO_2, 17.0% B_2O_3, 13.4% Na_2O, 1.8% ZrO_2, 4.0% Al_2O_3, <0.1% UO_2. This glass is representative of the cross-linked network of the glass developed in France to immobilize radioactive waste arising from spent fuel reprocessing.

Two 16 keV cascades were simulated in glass volumes of 526 847 atoms, as described in detail in a previous article [4]. A 25 keV displacement cascade was simulated in a cell containing 1 053 694 atoms.

The interactions between two atoms i and j separated by a distance r_{ij}, take the following form:

$$\phi_2(r_{ij}) = A_{ij}\exp\left(-\frac{r_{ij}}{\rho_{ij}}\right) + \frac{q_i q_j}{r_{ij}} - \frac{C_{ij}}{r_{ij}^6} + \frac{D_{ij}}{r_{ij}^8}. \quad (1)$$

The parameters were fitted to reproduce the overall structures as well as the local environments around the cations [11]. For the interactions around uranium atoms, the potential developed by Lindan and Gillan [12] was used for U–O interactions, while U-cation interactions were purely Coulombian.

Three-body terms were used to reproduce the angular orientation of the local environments induced by ionic-covalent bonds. These terms were of the form proposed by Stillinger and Weber [13] and the parameters applied to the aluminosilicate glass were based on work by Feuston and Garofalini [14].

$$\phi_3(r_{ij}, r_{ik}, \theta_{jik}) = \lambda\exp\left(\frac{\gamma_{ij}}{r_{ij} - r_c} + \frac{\gamma_{ik}}{r_{ik} - r_c}\right) \times \left(\cos\theta_{jik} - \cos\theta_0\right)^2, \quad (2)$$

where r_{ij}, r_{ik}, and θ_{jik} designate respectively the two internal distances and the angle of the triplet formed by a central atom i and two external atoms j and k; λ, γ and θ_0 are adjustable parameters. r_c is a cut-off radius beyond which the three-body terms vanish.

The parameter values of the potentials are indicated in Tables 1 and 2.

To shorten the computation time, we limited the Ewald sum to only its real component when simulating 16 keV and 25 keV cascades, with a large cut-off radius of 20 Å in real space. The greater efficiency of the CoMoD method allowed us to apply the complete Ewald sum to simulate the 70 keV cascade with a cutoff radius of 12 Å in real space.

Atoms approach one another during the ballistic collision sequence, resulting in strong instantaneous repulsion. These short-range interactions were represented by Ziegler–Biersack–Littmark (ZBL)

Table 1
Pair potential parameter values: A_{ij} (eV) and ρ_{ij} (Å)

	Si	O	B	Na	Zr	Al
A_{ij}						
Si	876.0	1045.1	353.5	903.6	2679.3	956.5
O		369.3	848.9	2996.3	4619.2	1725.3
B			126.8	392.6	1081.0	394.5
Na				882.4	2763.7	971.4
Zr					8194.8	2925.5
Al						1039.7
ρ_{ij}						
Si	0.29	0.328	0.29	0.29	0.29	0.29
O		0.35	0.29	0.316	0.29	0.29
B			0.29	0.29	0.29	0.29
Na				0.29	0.29	0.29
Zr					0.29	0.29
Al						0.29

The C_{ij} and D_{ij} parameters are zero except for O–Na pairs (C_{ij}(O–Na) = 453.7 eV Å^6 and D_{ij}(O–Na) = 544.5 eV Å^8).

Table 2
Adjustable parameter values λ_i (eV), $\gamma_{ij} = \gamma_{ik}$ (Å) and θ_0 for three-body terms

Parameter	O–Si–O, O–Al–O	Si–O–Si	O–B–O
λ_i (eV)	149.8	6.2	11985.0
$\gamma_{ij} = \gamma_{ik}$ (Å)	2.6	2.0	2.27
θ_0	109.47°	160.0°	109.47°

potentials [15]. Continuity of energy, force and force derivatives between ZBL potentials and Born–Mayer–Huggins potentials was ensured using fourth-order polynomials. Different cutoff radii were used depending on the relevant atom pair (see Table 3).

A cascade was initiated by accelerating a heavy projectile to a given energy. The projectile was first positioned at coordinates $Y = 0$, $Z = 0$ and $X = X_0$, then accelerated toward positive X values. All the atom positions were translated to conserve the relative distances between atoms, while ensuring that each atom remained inside the simulation cell.

Table 3
Cutoff radii for ZBL potentials ($r < r_{ZBL}$) and for pair potentials ($r > r_{BMH}$)

Pairs	r_{ZBL} (Å)	r_{BMH} (Å)
Si–B	0.7	1.1
Si–U, B–B	0.8	1.5
O–Na	0.8	1.4
O–U	1.1	1.3
Other	0.8	1.1

Fourth-order polynomial potentials are applied between the two.

Classic periodic conditions were applied during the calculation. A layer 3.5 Å thick was maintained at room temperature around the cell boundaries to ensure progressive dissipation of the thermal energy deposited by deceleration of the initial projectile.

The time step was adjusted throughout the cascade to avoid displacements exceeding 0.034 Å. Initially short, it was gradually lengthened (or shortened) according to variations in the highest instantaneous atom velocity. The hysteresis system described in reference [4] was used for this purpose.

2.2. Simulating cascades by the CoMoD method

The recently developed combined molecular dynamics (CoMoD) method allowed us to simulate cascades at realistic energies by breaking down the actual calculation into a set of elementary calculations. This method is based on coupling two types of molecular dynamics: short-range dynamics to predict the cascade morphology, and classical molecular dynamics. It has already been thoroughly described [9] and its application to a 70 keV cascade is detailed in an article recently published [10]. We will only mention the main features of the method here.

The calculation involves several steps. A glass containing several million atoms is initially fabricated by replicating a smaller unit cell in all three dimensions. A 64 000-atom cell replicated $5 \times 5 \times 5$ times in all three directions yields a simulation cell with 8×10^6 atoms.

The cascade morphology (defined as the set of all atoms displaced by more than 1 Å) is then computed using a molecular dynamics method simulating only interatomic collisions with short-range potentials (ZBL potentials extended by polynomials to reach zero potential beyond 1.35 Å). All the atoms are immobile at the end of this step. This approach very significantly accelerates the calculation of the ballistic portion of the cascade because of the short-range potentials; conversely, the glass structure relaxation after the ballistic collision sequence is not taken into account. At the same time, the local temperature variation is calculated on a mesh of unit cells 3.5 Å on a side.

The overall cascade morphology is then broken down into elementary zones, and for each zone the incoming projectiles and their entry direction

and energy are identified, as well as the thermal boundary conditions. It is thus possible by classic molecular dynamics to simulate the effect of these projectiles on each elementary zone through separate sets of independent calculations. Periodic conditions are applicable to the elementary zones via the artificial periodicity used to construct the simulation cell. The high-energy cascade (the ballistic collision phase followed by the structure relaxation phase) is thus fully simulated, unit volume by unit volume. The complete cascade can be reconstituted by adding together the partial calculations.

We validated the CoMoD method at low energy by satisfactorily reproducing calculations integrally performed using classical molecular dynamics. Some differences inevitably persist due to the chaotic nature of the ballistic collision phase. The method was then used at higher energy to simulate cascades ranging from 70 keV to 100 keV. The results obtained at high-energies (cascade volume, projectile path length, number of displacements, depolymerization peak) are fully consistent with what was observed between 0 keV and 25 keV.

A 70 keV cascade simulated by the CoMoD method will be used here to study damage variations in different regions of a cascade.

2.3. Identifying the cascade core region

In discussing the results, we will distinguish the core of the cascade from the peripheral zones. This distinction is based on several criteria.

2.3.1. Cylinder method

Cascades at energies of 16 keV or more extend along the path of the incident projectile, with a few branches corresponding to short subcascades. Therefore we used the incident projectile path to define a line from the initial projectile position to its final position (or the projectile entry and exit positions for each unit calculation by the CoMoD method).

Then we defined N different concentric cylinders with increasing radii in 15 Å increments, centered on this line and numbered from 1 to N. The smaller-diameter cylinders are closer to the core of the cascade, while larger-diameter cylinders correspond to more peripheral zones. Inside each cylinder, the variations over time of the atomic density, the degree of polymerization and the concentrations of different triplets can be analyzed to detect possible damage variations from one region to another.

2.3.2. Sphere method

Another way of delimiting the core of a cascade is to consider only individual displacements. Based on an earlier classification [3], four types of displacements characterize all the oxygen atoms displaced by more than 1 Å:

- individual displacements, corresponding to oxygen atoms with a coordination number of not less than 2 and for which all the neighbouring atoms were modified by the cascade; so around the new equilibrium site of an atom submitted to an individual displacement, the identities of the neighbouring atoms are completely modified;
- oxygen atoms for which the coordination number decreased from 2 to 1;
- collective displacements, corresponding to displaced oxygen atoms around which the neighbouring atoms remain unchanged; it means that the oxygen is displaced jointly with its neighbourhood;
- break-and-rebranch phenomena corresponding to oxygen atoms with coordination numbers of 2 or more around which only a fraction of the neighbouring atoms were modified.

Individual displacements and coordination transitions from 2 to 1 occur more frequently during the initial instants of the cascade, whereas collective displacements and break-and-rebranch phenomena occur later on average.

Fig. 1 shows the spatial distribution of displacement types during a 25 keV cascade. For each displacement, we calculated the distance between the position of the displaced atom and the cascade centerline. Each curve is based on the total number of

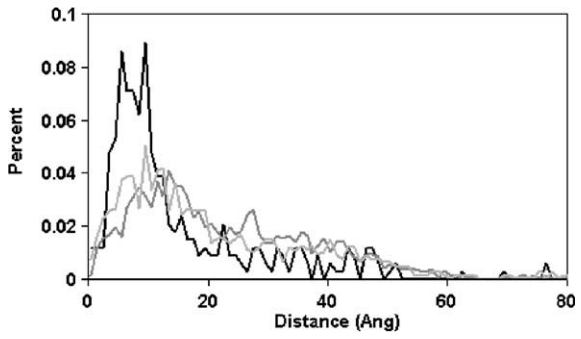

Fig. 1. Normalized distance distributions between 25 keV cascade centerline and different types of displacements: individual displacements (black), collective displacements (dark gray), and break-and-rebranch phenomena (light gray).

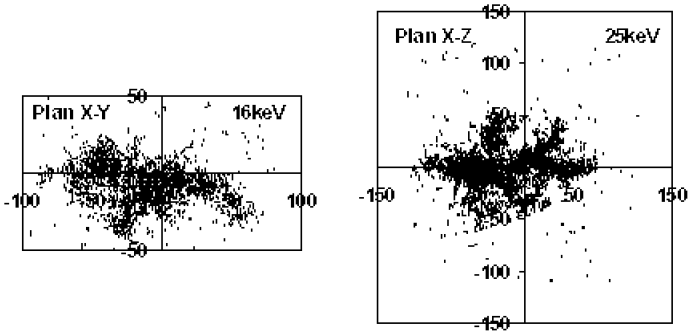

Fig. 2. Morphology of a 16 keV cascade (left) and a 25 keV cascade (right) simulated by classical molecular dynamics. For clarity, only the oxygen atoms displaced by more than 1 Å are shown. Coordinates are in Å.

displacements of a particular type (i.e. the *Y*-axis refers to percentages). A high-amplitude peak related to individual displacements is visible at a distance of 7.5 Å, while the peaks on the curves for the other types of displacements are slightly shifted and cover a broader range of distances. The set of individual displacements will therefore be used as a rough delimiter of the core region of the cascade.

Around each individual displacement, concentric spheres of increasing radii are defined in 5 Å increments, inside which the atomic density, degree of polymerization and triplet concentrations are calculated. This approach can also be used to probe the cascade core region and establish damage variations between the core and the periphery.

3. Results

3.1. General analysis of recoil nucleus effects

3.1.1. 16 keV and 25 keV Cascades simulated by classical molecular dynamics

Two 16 keV cascades and a 25 keV cascade initiated by a heavy nucleus were simulated by classical molecular dynamics. Two cascade morphologies are shown in Fig. 2. In both cases, the relatively linear projectile path is visible with a few short branching subcascades.

In the remainder of this paragraph, we will quantitatively describe only the 25 keV cascade; the results obtained for the 16 keV cascades were qualitatively identical.

The variation over time of the displacements by species and of the depolymerization index for the 25 keV cascade are indicated in Figs. 3 and 4. The degree of depolymerization is determined by continually calculating the differences between the

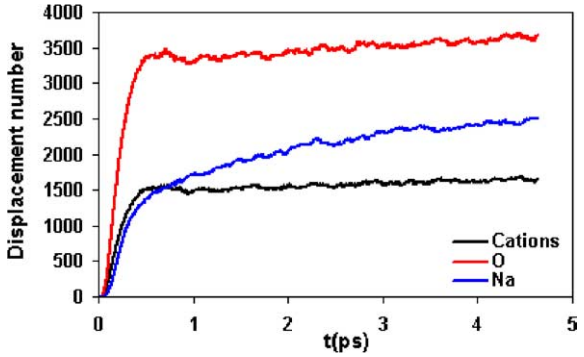

Fig. 3. Displacements versus time for various species (atoms displaced by more than 1 Å) during the 25 keV cascade.

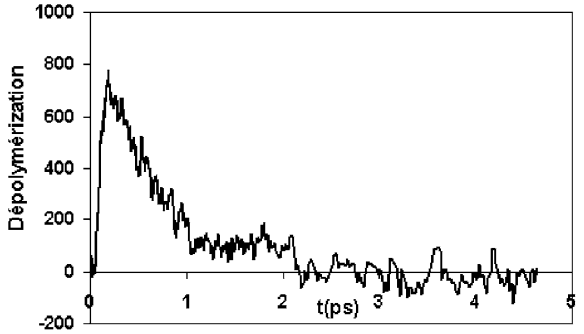

Fig. 4. Degree of depolymerization versus time during the 25 keV cascade.

instantaneous coordination numbers and initial coordination numbers of Si, B and Al. The sum of the differences, i.e. the number of chemical bonds broken at any given instant, defines the depolymerization index. A positive index corresponds to a decrease in the number of chemical bonds (the differences are calculated between the initial and final coordination numbers).

Table 4
Distribution of oxygen atom displacements according to the classification described in Section 2.3.2 for a 25 keV cascade

Type	Percentage
Individual displacements	7.3
Coordination number $2 \rightarrow 1$	3.4
Collective displacements	43.8
Break-and-rebranch	32.4

The characteristics of the 25 keV cascade are consistent with lower-energy cascades, not only for the number of displacements and for the height of the depolymerization peak prior to glass structure recovery, but also for the distribution of the different types of oxygen displacements. Table 4 shows the percentages of oxygen atom displacements according to the classification defined in a previous article [3] and mentioned above. It confirms the predominance of collective displacements and break-and-rebranch phenomena over individual displacements and oxygen atoms for which the coordination number diminished from 2 to 1.

Fig. 5 shows the distance distributions according to the type of displacement. Individual displacements correspond to longer paths, as they involve higher energies. During this 25 keV cascade, displaced oxygen atoms accounted for 47.7% of the total, compared with 30.7% for displaced sodium atoms; these percentages are consistent with previous results at lower energies [4].

The behaviour of the sodium atoms reproduces earlier observations in that they once again occupy peripheral positions in the cascade morphology [4]. The length of the displacements slightly exceeds that of the oxygen and network forming atoms.

The internal pressure variation at the end of the 25 keV cascade results in 0.113% relative swelling of the simulation cell at the end of the 10 ps cascade.

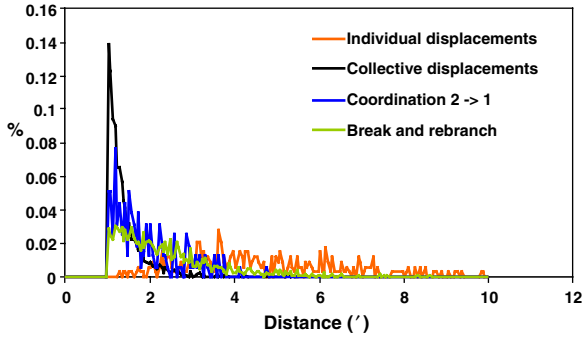

Fig. 5. Displacement distance distribution per type.

This value was determined by assuming a bulk modulus of 115 GPa, and corresponds to absolute swelling of 15.3 nm^3 for a cell measuring about 13 500 nm^3. The relative swelling is therefore only indicative, but has no absolute meaning in so far as it is highly dependent on the ratio between the simulation cell size and the volume occupied by the cascade. In addition, the swelling due to the cascade itself is augmented by a temperature effect, as the final specimen temperature after 10 ps still exceeds the initial temperature by 90 K. Extrapolating the pressure curve to room temperature results in a negative internal pressure variation, i.e. a slight contraction, concomitant with the increasing polymerization index. The differences remain small, however, and simply highlight the fact that the variations in polymerization and internal pressure are merely anecdotal.

3.1.2. 70 keV cascade simulated by the CoMoD method

The 70 keV cascade morphology is shown in Fig. 6. Once again the initial projectile track is highly visible, as are the branching subcascades. This cascade has already been described in detail in reference [10].

The number of displacements and the height of the depolymerization peak are collinear with the results obtained at lower energies; this allows the

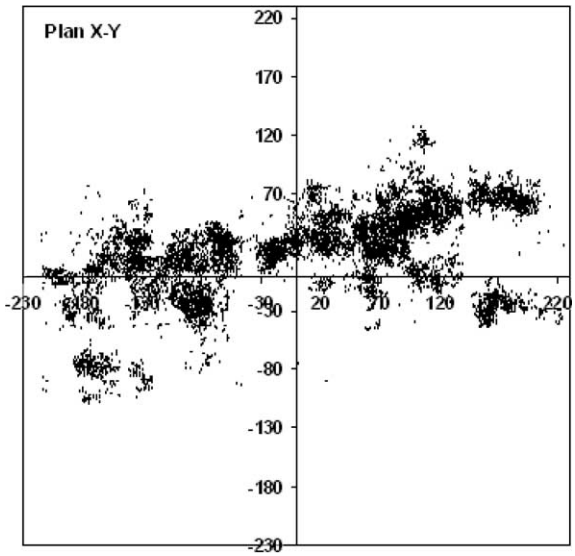

Fig. 6. Morphology of a 70 keV cascade. Only oxygen atoms displaced by more than 1 Å are shown. Coordinates are in Å.

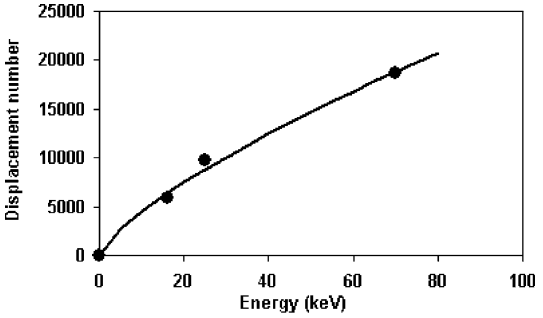

Fig. 7. Number of displacements versus incident projectile energy. The solid curve represents the trend line for Eq. (3).

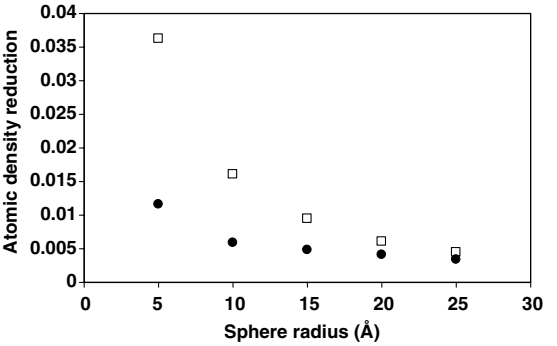

Fig. 8. Atomic density variation around individual (□) and collective (●) displacements for a 25 keV cascade. See the text for the definition of the atomic density variation unit.

number of displacements N_{disp} to be expressed as a function of the energy as follows:

$$N_{\text{disp}} = 824.5 \times E^{0.74} \ (E \text{ in keV}). \tag{3}$$

The numerical results and parameter fitting curve are shown in Fig. 7. The order of magnitude of the power coefficient corresponds to the value determined in various metals and crystalline oxides [16,17].

The height of the depolymerization peak preceding the glass structure recovery phase is given by the following formula:

$$H = 41.4 \times E^{0.89} \ (E \text{ in keV}), \tag{4}$$

where H represents the maximum number of broken bonds prior to structure recovery.

The parameters of Eqs. (3) and (4) should be considered with an appreciable error margin because of the small number of points on which they were determined.

The final depolymerization of the 70 keV cascade, averaged over the last few picoseconds, corresponds to some fifty broken bonds. The broken bonds are situated mainly in the cascade periphery, where thermal annealing was not intense enough to restore the glass structure. The increasing recovery of a zone as the incident projectile energy increases was demonstrated in an earlier article [10] and will not be discussed again here.

3.2. Local analysis of the effect of the recoil nucleus: damage in the cascade core region

3.2.1. 25 keV cascade

We will consider only the 25 keV cascade here, given that similar results were obtained for both 16 keV cascades.

Around each individual and collective displacement we plotted concentric spheres with radii of 5, 10, 15, 20, and 25 Å. Inside each sphere, we calculated the number of atoms and the degree of polymerization at the initial and final instants. The degree of polymerization is defined as the sum of the coordination numbers of the Si, B and Al atoms.

Fig. 8 shows the mean variations in the number of atoms for each of the spheres divided by the volume of the sphere, i.e. the variation of the local atomic density expressed as the number of atoms per unit volume. A positive value corresponds to a density reduction (the variation is calculated as the initial value less the final value).

The result indicates a systematic density reduction that is more significant for individual displacements than for collective displacements, and becomes less significant as the spherical radius increases.

The density variations around the collective displacements are substantially lower – by about a factor of 3. The final variations stabilize at about 5×10^{-3}, no doubt because of the temperature variation. A nonzero residual density variation could persist since the temperature around the final displacement positions is higher than the initial temperature.

Fig. 8 proves that structural damage is concentrated around the individual displacements, i.e. where the collisions were violent enough to break the bonds. Collective displacements occur only near the end of the collision sequences, when the energies are no longer sufficient to break the bonds. We were unable to detect any correlation between the intensity of the density variation and the distance covered

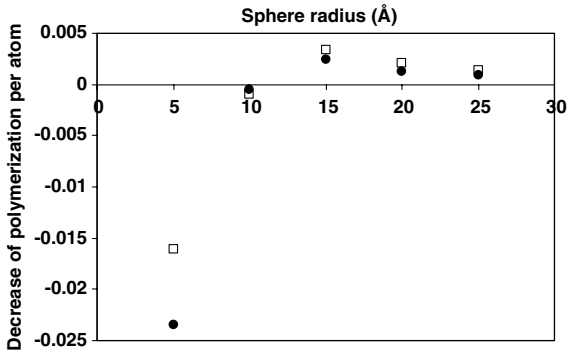

Fig. 9. Variation of degree of polymerization per atom around individual (□) and collective (●) displacements. Refer to text for a definition of the degree of polymerization per atom. The differences are noted between the initial and final values.

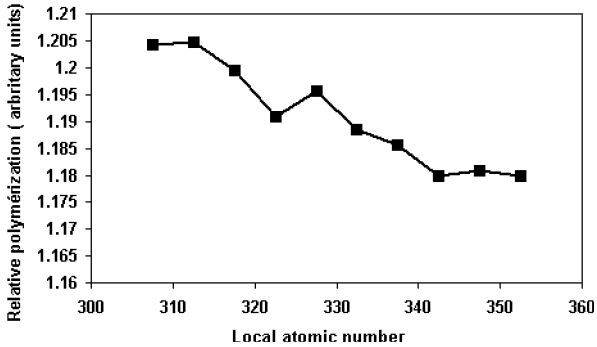

Fig. 10. Polymerization per atom versus local atomic density in an unirradiated glass structure. Refer to text for the calculation method.

by the individually displaced atom because of the very scattered data points.

Fig. 9 shows the variations in the degree of polymerization normalized by the number of atoms in the sphere surrounding individual and collective displacements; i.e. we divided the initial degree of polymerization by the number of atoms initially present in the sphere, and the final degree of polymerization by the final number of atoms. This figure thus indicates the degree of polymerization per atom, expressed by the variation between the initial and final values, so a positive value indicates a decrease in the polymerization per atom. The degree of polymerization is always calculated as the sum of the coordination numbers of the Si, B and Al atoms contained in a given sphere.

Significant variations are observed only in the first sphere. The total number of chemical bonds, i.e. the degree of polymerization, diminished in absolute value due to the drop in the number of atoms (curve not shown). But when the degree of polymerization is expressed in terms of the local atom density (Fig. 9), the degree of polymerization per atom actually increases (the points corresponding to the 5 Å radius sphere are negative). The intensity of this phenomenon is roughly identical around the collective and individual displacements; this implies that local reconstruction, which requires only local atom movements, is just as effective around both types of displacements, irrespective of the instantaneous collision intensity.

This raises the issue of the relationship between the local density of a glass and its degree of polymerization per atom. In Fig. 10 we have plotted the degree of polymerization per atom versus the number of atoms for grid of 1000 spheres with a 10 Å radius, thus probing the entire glass structure of 10^6 atoms. For each data point with coordinates (x, y) in Fig. 10, y corresponds to the polymerization per atom averaged over all the spheres in which the number of atoms is contained within the interval $[x - 2.5; x + 2.5]$. It is clear that, as the local number of atoms decreases, the polymerization per atom increases. The joint variation of the local density and the polymerization per atom observed following the passage of a projectile in the structure is thus not an effect proper to irradiation, but a general structural effect. There is a natural correlation in a glass structure between a low local atomic density and a high degree of polymerization per atom.

In order to further clarify the issue of the glass behaviour according to the position of the perturbation with respect to the cascade morphology, we plotted the variation in the number of atoms inside the spheres surrounding individual displacements versus the distance between the individual displacement and the initial projectile position (Fig. 11).

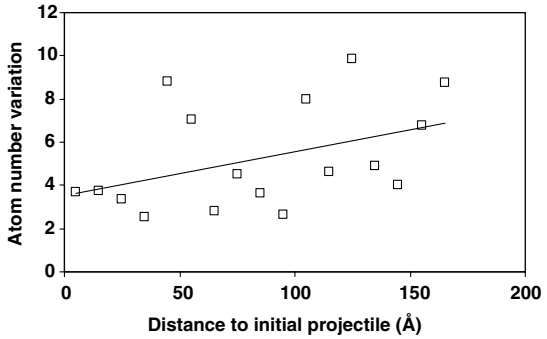

Fig. 11. Variation of the number of atoms around individual displacements versus the distance between individual displacement and initial projectile position.

Once again, the variation in the number of atoms was averaged over 10 Å distance increments to limit the fluctuations from one point to another. A positive value corresponds to a decrease of the number of atoms.

We have also added a trend line for the data points in Fig. 11. The number of atoms appears to decrease more and more with the distance from the initial projectile position, despite considerable fluctuations from one point to the next. This trend again suggests better average annealing near the initial projectile position, i.e. in the regions subjected to the greatest local heating. Nevertheless, even in the immediate vicinity of the initial projectile position, the variation in the number of atoms is not nil: there is a persistent residual deficit, here again probably related to the temperature that has not returned to room temperature at the end of the cascade.

Defining concentric cylinders along the projectile track also allowed us to measure variations in the number of atoms and their spatial extent. Fig. 12 shows that the number of atoms decreases in the first two cylinders (a positive value corresponds to a decrease of the atomic density), i.e. within 15 Å around the projectile track.

Each point in Fig. 12 was calculated by first measuring the difference between the initial and final number of atoms in a cylinder, then dividing the difference by the number of atoms initially present. Beginning with the third cylinder, the variation in the number of atoms as a percentage of the initial number of atoms becomes negligible.

The central cylinder with a radius of 15 Å was then divided lengthwise into segments 10 Å long,

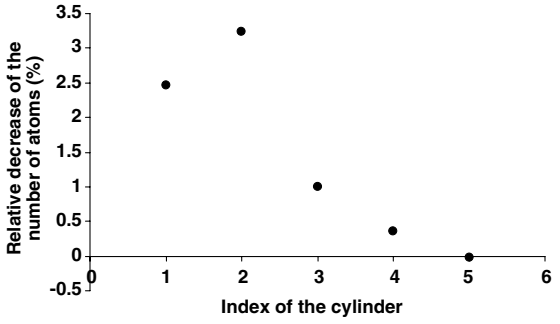

Fig. 12. Relative variation in the number of atoms in concentric cylinders around the 25 keV projectile path. Cylinder 1: 5 Å radius; cylinder 2: radius between 5 Å and 15 Å; cylinder 3: radius between 15 Å and 30 Å; cylinder 4: radius between 30 Å and 45 Å; cylinder 5: volume beyond 45 Å radius.

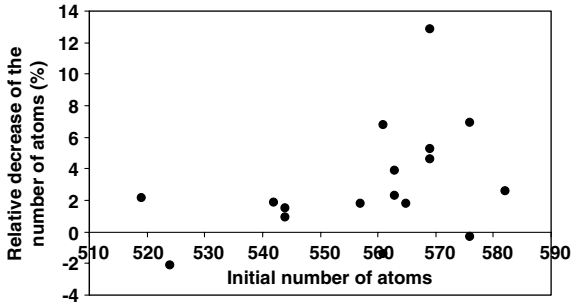

Fig. 13. Relative variation in the number of atoms in each 10 Å long segment of a cylinder with a 15 Å radius centered on the 25 keV projectile path.

and the variation in the number of atoms was plotted for each segment (Fig. 13). Each point corresponds to the difference between the initial and final number of atoms in a given segment divided by the initial number of atoms, i.e. expressed as a percentage of the initial number of atoms. In the segments with a low initial atomic density, the number of atoms did not diminish. The most significant decreases were observed for segments in which the initial atom population was already high. This curve shows that the structure is characterized by a minimum local atomic density threshold.

A local analysis of the damage arising from a 25 keV cascade thus reveals a relatively complex relation between the local damage intensity and the position within the cascade morphology. The damage is most intense around individual displacements, but with better annealing in the hottest regions. A second correlation is observed between the initial atomic density and the damage intensity, which is highest in regions of high initial atomic density.

3.2.2. 70 keV cascade

The 70 keV cascade was calculated using the CoMoD method, i.e. by breaking down the overall calculation into a series of elementary calculations in smaller cells. As for the 25 keV cascade, we analyzed the changes in the atomic densities at each calculation step using the concentric cylinder method.

The morphology of each elementary calculation step was different, and the cylinder positions had to be redefined in each case. Fig. 14 shows a typical example of cylinder positioning. It was not always easy to identify a clearly defined track, and it was impossible to position a cylinder around two of the eleven zones defined to simulate the 70 keV

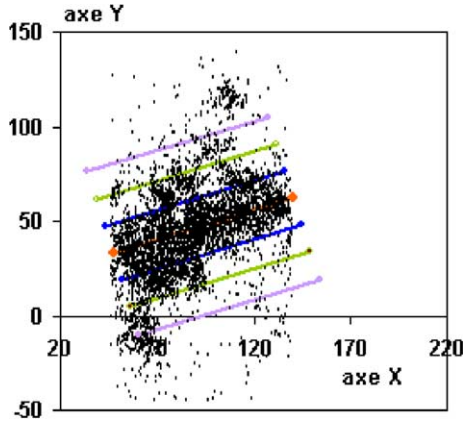

Fig. 14. Example of cylinders positioning for analysis of atomic density variations during a 70 keV cascade simulated zone-by-zone. Lines represent concentric cylinders with radii of 15 Å, 30 Å and 45 Å. Coordinates are in Å.

cascade. Conversely, two series of cylinders were plotted in zone 3, which contained a clearly visible subcascade.

Having defined a set of cylinders surrounding the regions damaged by the cascade, we then calculated the difference between the initial and final number of atoms in each cylinder of 15 Å radius, and divided the difference by the initial number of atoms to obtain the percentage variation in the number of atoms for each cylinder.

The bell curve in Fig. 15 shows the relative variations versus the energy of the highest velocity projectile entering the zone containing the cylinder. The atom populations vary only slightly at low and very high energies; the maximum effect occurs over a relatively broad range roughly from 10 keV to 25 keV.

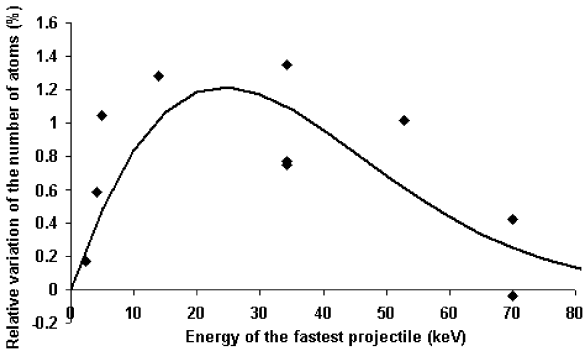

Fig. 15. Relative variation in the number of atoms in central cylinders (15 Å radius) defined over calculation zones for the 70 keV cascade versus the energy of the highest-velocity incoming projectile. The solid curve represents the bell-shaped distribution of the scatter plot.

A trend line was plotted in Fig. 15 to highlight the nonlinearity of the damage in the cascade core region versus the local collision intensity. The regions struck by the projectiles with the highest velocities are annealed to a state closer to the pristine state; the regions struck by low-energy projectiles are relatively undisturbed, and between the two lies the zone of maximum damage.

As the energy increases, the increasing damage begins to outweigh structure annealing. The situation is then reversed: above a given energy threshold, structure annealing prevails over the damage induced by the projectiles, with virtually complete annealing near 70 keV.

4. Discussion

A body of evidence supports our contention that damage within the cascade morphology is variable depending on the local energies of the projectiles. Consistent results were obtained from 16 keV, 25 keV and 70 keV cascades.

The relative damage increases as long as the local projectile energy remains below about 10 keV. At higher energies the relative variation in the number of atoms levels off, indicating that annealing by thermal agitation is starting to become effective. Above 25 keV and up to 70 keV, annealing becomes increasingly effective and the relative variations in the number of atoms continue to diminish.

Damage thus accumulates in regions of intermediate projectile energy between the initial high energy of the main projectile and low-energy regions at the tail end of the cascade. These regions remain confined within cylinders of about 15 Å radius centered on the paths of the highest velocity projectiles.

The relationship between the density variation and depolymerization is not as obvious as first expected. On the whole, variations in the degree of polymerization are limited: some fifty chemical bonds were broken during the 70 keV cascade, and about 20 bonds were reformed during the 25 keV cascade. Locally, however, the relative variations in the degree of polymerization are more complex.

The absolute polymerization (the number of chemical bonds) decreases mechanically with the local atomic density because the number of atoms decreases, but the polymerization per atom (the mean number of chemical bonds involving network formers) increases slightly as the local atomic density diminishes. The greater degree of freedom associated with the local decrease in the number of

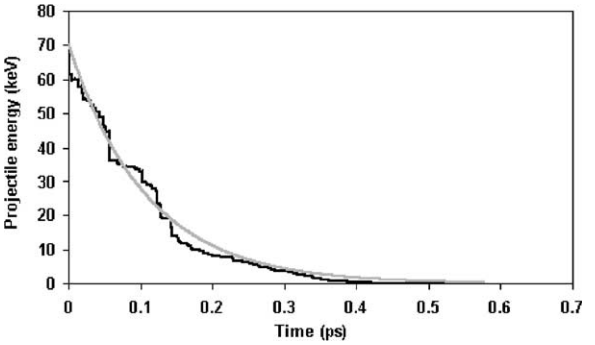

Fig. 16. Main projectile energy versus time during a 70 keV cascade. The gray curve represents the fit using Eq. (5).

atoms no doubt favours the formation of new bonds.

The polymerization index is thus useful in general – as long as the number of atoms is constant – for estimating the changing connectivity of a glass structure subjected to the impact of a projectile, but becomes more difficult to apply as a local damage probe when the number of atoms is subject to local variations.

Fig. 16 plots the decreasing projectile velocity versus time for the 70 keV cascade. We fitted the curve with an expression of the following type:

$$E = E_0 \exp(-At). \tag{5}$$

Let $v(t)$ be the projectile velocity at time t. During the time interval $\mathrm{d}t$, the projectile will cover a distance $\mathrm{d}x = v(t) \cdot \mathrm{d}t$ and will deposit locally an energy density $\mathrm{d}E/\mathrm{d}x$ given by the relation:

$$\frac{\mathrm{d}E}{\mathrm{d}x}(t) = \frac{AE_0 \exp(-At)}{v(t)}. \tag{6}$$

The locally deposited energy depends on the instantaneous projectile energy; it is plotted in Fig. 17 for the 70 keV cascade, gradually decreasing from the initial value as the projectile velocity diminishes. It is difficult to specify a thermal equivalent for the deposited energy, as this would require knowledge of the exact volume in which the energy is dissipated. Nevertheless, the higher the instantaneous projectile velocity, the greater the local heating; this accounts for the existence of a threshold (about 10 keV) above which the local heating becomes sufficient to begin annealing the damage caused by interatomic collisions.

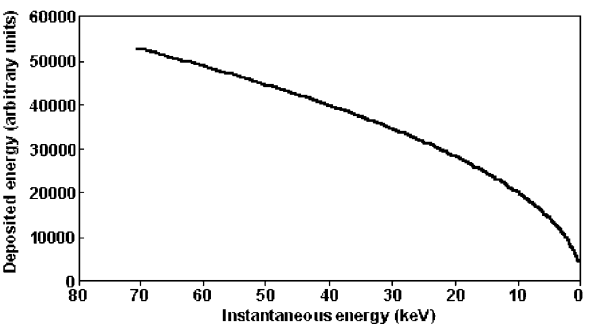

Fig. 17. Locally deposited energy versus instantaneous projectile energy for a 70 keV cascade.

Local atomic density variations due to the impact of a heavy projectile are inhomogeneous in two respects. As noted above, the density variations on average are greater in the intermediate regions between the initial projectile position and either end of the cascade. In addition, Fig. 13 indicates that the higher the initial density, the greater the local density reduction. There appears to be a lower density limit of about 0.0778 atom/Å^3 below which the density no longer diminishes.

The existence of this limit is no doubt related to the saturation of experimental swelling at about 0.6% for the French nuclear glass doped with short-lived actinides [18]. In the segments analyzed along the 25 keV projectile path, the relative mean swelling was 2.7% with major discrepancies ranging from −2.3% to 12.8%, confirming the highly scattered local density variations. It is very difficult to estimate a macroscopic swelling value for a given dose based on these local variations.

It is interesting to compare our results with those of leaching experiments on borosilicate glass with high boron concentrations doped with 4 wt% ThO_2 and short-lived actinides [19]. These specimens have integrated decay from ^{232}Th for 17 years. The ^{232}Th decay chain leads to the formation of ^{228}Th. Comparing the ^{228}Th and ^{232}Th release shows that the former is leached in greater amounts when the glass is placed in contact with a solution; this implies that ^{228}Th (which logically occupies the ends of the recoil nuclei tracks) enters solution more readily than its precursors.

The atomic density variations observed in the recoil nuclei tracks by molecular dynamics might well account for the results of this experiment, assuming the regions of lower local density are more readily leached. This hypothesis is not unreasonable in so far as the lower-density regions in the atomic lattice might allow easier access to water molecules and thus facilitate dissolution. Locally deficient atomic densities could thus accelerate the leaching of daughter radionuclides.

We have assumed here that our simulation results are also applicable to highly borated glasses.

The inhomogeneity of damage and local annealing within a cascade is interesting, and is no doubt also the case for other crystalline or amorphous oxide or metallic matrices.

This observation could suggest changes in models used to predict defect concentrations according to the projectile energy. Current models (NRT [5,20] or Kinchin and Pease [21]) take defect annealing into account by means of an additional factor, κ, with a value near 0.8 for the NRT model.

The nonlinear relation between the local damage and the local projectile energy implies that κ is not a constant, but instead depends on the local projectile energy. The existing model integrates the $n(T,E)$ function, which corresponds to the density of atoms accelerated to the kinetic energy interval T to $T+\mathrm{d}T$, between two limits E and L corresponding to the initial projectile energy and the displacement multiplication threshold energy, respectively. The total number of displacements $N_{\mathrm{D}}(E)$ is thus expressed as

$$N_{\mathrm{D}}(E)=\int_{L}^{E} n(T,E)\,\mathrm{d}T. \tag{7}$$

In the current formulation:

$$n(T,E)=\frac{cE}{T^2} \tag{8}$$

hence:

$$N_{\mathrm{D}}(E)=\frac{cE}{L} \tag{9}$$

and the number of Frenkel pairs is:

$$N_{\mathrm{F}}(E)=\frac{cE}{L}\kappa \tag{10}$$

with κ taking into account the atoms that have returned to an equilibrium site during the cascade.

Our observations suggest that the κ constant should be replaced by a function $\kappa(T)$ dependent on the locally deposited energy. The equation predicting the number of defects would then become:

$$N_{\mathrm{F}}(E)=\int_{L}^{E} n(T,E)\kappa(T)\,\mathrm{d}T. \tag{11}$$

A statistical study of local defect concentrations within the cascade morphology should allow to specify a function $\kappa(T)$ that decreases when T increases to take into account the improved damage annealing and thus refine predicted defect concentrations according to the energy of the incident projectile.

5. Conclusion

Displacement cascades at energies ranging from 16 keV to 70 keV were simulated by classical molecular dynamics. Damage inhomogeneity was observed in each case: the atomic density was diminished by the incident projectile to a variable extent depending on the regions concerned. The regions near the initial projectile position are largely annealed, and regions near the end of the cascade are relatively unaffected because of the low residual projectile energy. However, maximum damage occurs in intermediate regions from collisions with incident projectiles at energies ranging from about 10 keV to 25 keV.

This phenomenon illustrates the competition between structure annealing and projectile-induced damage; both increase with the local energy, but with different dynamics. At the highest energies, annealing wins out over damage, restoring the glass structure to its pristine state; hence the good structural behaviour in the zones closest to the initial projectile position, which are subjected to the greatest local temperature rise.

This work also reveals the complex relationship between the local atomic density and the degree of polymerization. Although the absolute degree of polymerization decreases with the local atomic density, the degree of polymerization per atom increases, probably as a result of the greater degree of freedom available to the structure.

The damage inhomogeneity in the core region of displacement cascades suggests to refine the current models used to predict the number of atomic displacements (NRT, Kinchin–Pease) by considering an annealing factor $\kappa(T)$ dependent on the locally deposited energy T.

References

[1] W.J. Weber, R.C. Ewing, C.A. Angell, G.W. Arnold, A.N. Cormack, J.-M. Delaye, D.L. Griscom, L.W. Hobbs, A. Navrotsky, D.L. Price, A.M. Stoneham, M.C. Weinberg, J. Mater. Res. 12 (1997) 1946.
[2] Y. Adda, A. Barbu, G. Brebec, N.V. Doan, R. Gupta, Y. Limoge, B. Perraillon, P. Regnier, Y. Serruys, Ann. Chim. Fr. 10 (1985) 499.
[3] J.-M. Delaye, D. Ghaleb, Phys. Rev. B 61 (2000) 14481.
[4] J.-M. Delaye, D. Ghaleb, J. Non-Cryst. Solids 330 (2003) 106.
[5] M.T. Robinson, J. Nucl. Mater. 216 (1994) 1.
[6] M.P. Allen, D.J. Tildesley, in: M.P. Allen, D.J. Tildesley (Eds.), Computer Simulation in Chemical Physics, Kluwer Academic Publishers, 1993.

[7] T. Diaz de la Rubia, G.H. Gilmer, Phys. Rev. Lett. 74 (1995) 2507.
[8] R.S. Averback, T. Diaz de la Rubia, Solid State Phys. 51 (1997) 282.
[9] J.-M. Delaye, D. Ghaleb, Phys. Rev. B 71 (2005) 224203.
[10] J.-M. Delaye, D. Ghaleb, Phys. Rev. B 71 (2005) 224204.
[11] J.-M. Delaye, L. Cormier, D. Ghaleb, G. Calas, J. Non-Cryst. Solids 293–295 (2001) 290.
[12] P.J.D. Lindan, M.J. Gillan, J. Phys. Condens. Matter 3 (1991) 3929.
[13] F.H. Stillinger, T.A. Weber, Phys. Rev. B 31 (1985) 5262.
[14] B.P. Feuston, S.H. Garofalini, J. Chem. Phys. 89 (1988) 5818.
[15] J.F. Ziegler, J.P. Biersack, U. Littmark, The Stopping Range of Ions in Matter, Pergamon, New York, 1985.
[16] D.J. Bacon, F. Gao, Y.N. Osetsky, Phys. Res. B 153 (1999) 87.
[17] L. Van Brutzel, J.-M. Delaye, D. Ghaleb, M. Rarivomanantsoa, Phil. Mag. 83 (2003) 4083.
[18] Hj. Matzke, E. Vernaz, J. Nucl. Mater. 201 (1993) 295.
[19] Y. Eyal, R.C. Ewing, in: D. Alexandre, R. Baker, R. Kohout, J. Marek (Eds.), Proceedings of the International Conference on Nuclear Waste Management and Environmental Remediation, Vol. 1, ASME, New York, 1993, p. 191.
[20] M.J. Norgett, M.T. Robinson, I.M. Torrens, Nucl. Eng. Des. 33 (1975) 50.
[21] G.H. Kinchin, R.S. Pease, Rep. Prog. Phys. 18 (1955) 1.